Macromolecules

ARTICLE

pubs.acs.org/Macromolecules

Synthesis of Well-Defined Photo-Cross-Linked Polymeric Nanocapsules by Surface-Initiated RAFT Polymerization

Xin Huang,* Dietmar Appelhans,* Petr Formanek, Frank Simon, and Brigitte Voit

Leibniz Institute of Polymer Research Dresden, Hohe Strasse 6, 01069 Dresden, Germany

Supporting Information

ABSTRACT: Narrowly distributed hollow polymeric nanocapsules (PtBMA-*co*-PDMIPM-*b*-PHPMA), with the size of 450 or 900 nm, were first synthesized by surface-initiated reversible addition−fragmentation chain transfer (RAFT) polymerization exploiting silica nanoparticles as sacrificial templates and 2,3-dimethylmaleic imidopropyl methacrylate (DMIPM) as a photo-cross-linker. First, silica nanoparticles were amino functionalized by aminosilane agents, and then the dithiocarbonate chain transfer agent (CTA) was anchored via activated R-groups to the amino-functionalized surface of silica nanoparticles. This surface layer of CTA groups was then used to grow linear copolymers and block copolymers by RAFT polymerization leading to a core−shell morphology. TEM and GPC results indicated that the thickness of the shell can be well governed by simply controlling the molecular weight of the grafted copolymer. Finally, after photo-cross-linking and etching the silica core with NH_4F/HF buffer, hollow nanocapsules were obtained, of which the morphology and composition were confirmed by employing a range of techniques, such as TEM, cryo-TEM, DLS, SEM, XPS, TGA, FTIR, GPC, and UV−vis spectroscopy. Thus, robust and narrowly distributed polymeric nanocapsules with size of 450 nm and a wall thickness 10 nm based on the grafted block copolymer PtBMA-*co*-PDMIPM-*b*-PHPMA having M_n = 19 500 g/mol (GPC) could be prepared.

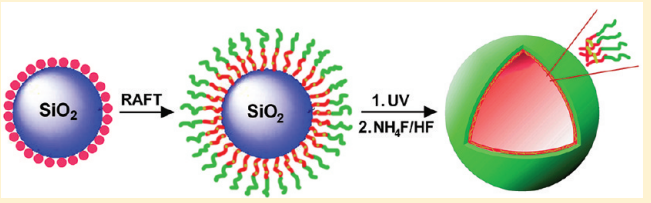

INTRODUCTION

Hollow nanocapsules with an empty core domain and a polymer shell have recently attracted considerable attention due to their unique properties including encapsulation capability, controllable surface permeability, and surface functionality.[1−3] Such hollow polymeric spheres have been proven to possess wide applications in many fields, including catalysis, controlled drug-delivery systems, artificial cells, nanoreactors, and photonic crystals.[4−10] To date, various routes leading to hollow particle morphologies have been explored,[11−16] such as emulsion polymerization,[17] phase separation,[18] cross-linking of micelles,[19] or a directed self-assembly method.[20−22] Among them, the colloidal templating method, involving the coating of a sacrificial inorganic/organic template with polymer followed by stabilization of the polymer shell via a cross-linking reaction, is especially popular.[23,24] The template is typically selected to be a readily removable inorganic nanoparticle, e.g., made from silica or gold. Thus, by combining this method with layer-by-layer (LBL) technique, Caruso et al. offered an elegant, simple, and versatile route to form polymeric capsules with tailored properties for biomedical applications.[25]

Recently, surface-initiated living radical polymerization (LRP)[26−28] has been rapidly developed for its excellent controllability of the molecular weight and polydispersity of the graft polymers and its capability of affording an exceptionally high grafting density with the robustness and versatility of LRP retained. This technique has been successfully applied to synthesize polymer brushes on a variety of solid surfaces including flat substrates,[29,30] fine particles,[31−38] and porous[39] or tubelike structures.[40,41] Very recently, strategies focused on tailoring silica nanoparticle (SNP) surfaces with polymers by surface-initiated LRP techniques to prepare hollow nanocapsules have also been described.[8,42−50] So, by surface-initiated atom transfer radical polymerization (ATRP), an oxetane-functionalized block copolymer was built on the surface of SNP. Making use the ring-opening reactivity of oxetane for the shell cross-linking and dissolving the core, a monodispersed hollow nanocapsule was reported by Fukuda et al.[51] Also based on this surface-initiated ATRP method, Kang et al. prepared a block copolymer of PS-*b*-PMMA grafted SNP.[49] Ultraviolet exposure of the hybrid particles resulted in cross-linking of the PS intermediate layer and decomposition of the PMMA outermost layer, and subsequent removal of the silica core with HF etching provided cross-linked PS hollow nanocapsules. Additionally, recently some work focused on surface-initiated distillation−precipitation polymerization by anchoring vinyl monomer onto silica surfaces to produce hollow nanocapsules.[43,44,46,48] However, compared with the extensively used reversible addition−fragmentation chain transfer (RAFT) polymerization to synthesize various polymer architectures, there are surprising few reports based on the surface-initiated RAFT polymerization to synthesize hollow nanocapsules. Only very recently, a RAFT-based vesicle-templating approach to synthesize the polymeric nanocapsules was reported by Ali et al.[52]

Received: August 30, 2011
Revised: September 28, 2011
Published: October 11, 2011

Scheme 1. General Procedure for the Synthesis of the Photo-Cross-Linked Nanocapsules

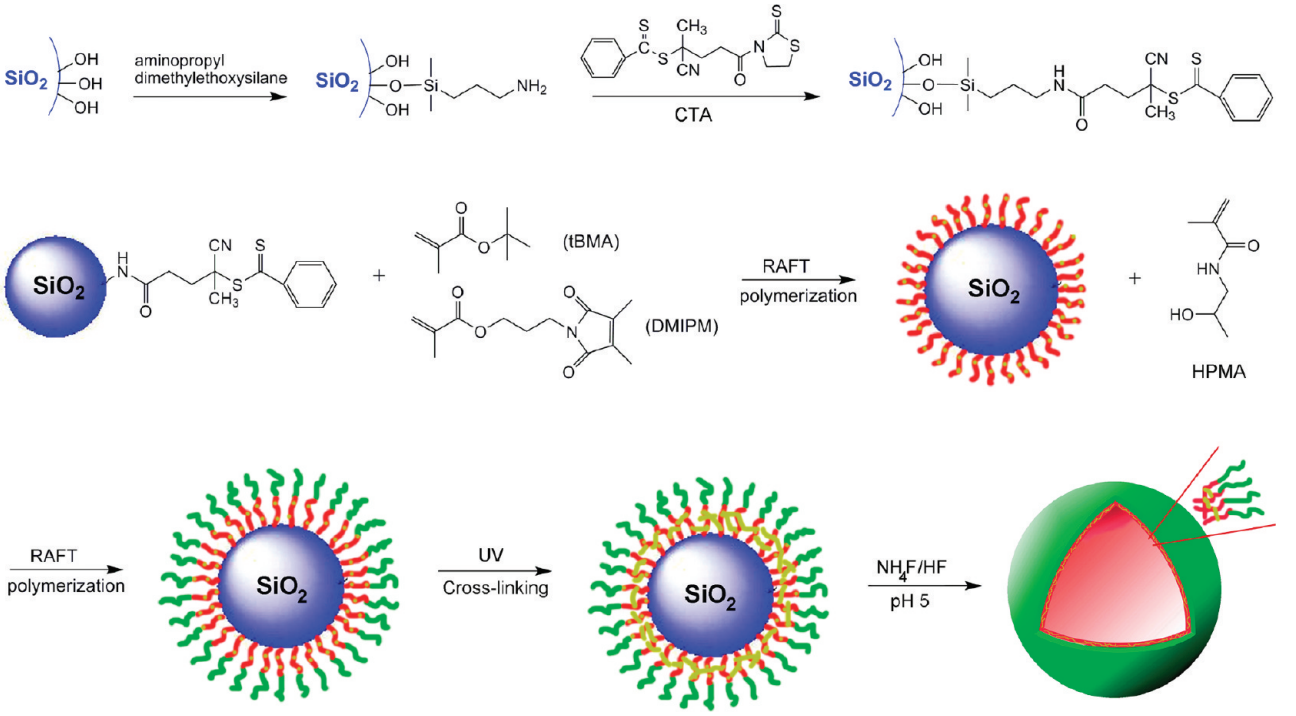

Scheme 2. Synthetic Routes of R-Group Activated CTA

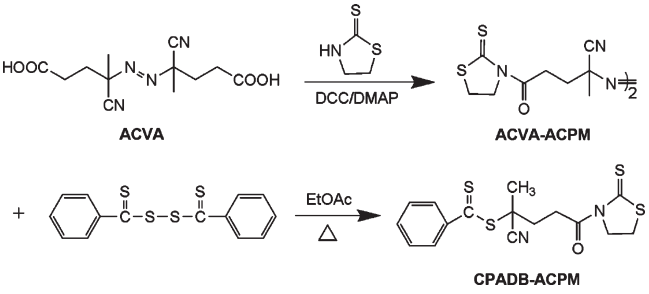

Reversible addition−fragmentation chain transfer (RAFT) has emerged as a promising controlled radical polymerization technique due to its versatility and simplicity and the advantage that the resulting polymer is free from the contamination of metal catalyst.[53−59] Also, RAFT is compatible with almost all of the conventional radical polymerization monomers. Taking advantage of this polymerization technique, after anchoring CTA onto silica nanoparticles, different polymer brushes based on silica nanoparticles are reported by Benicewicz,[60,61] Brittain,[62,63] Zhao,[64,65] Pan,[66] and Perrier et al.[67]

Inspired by these works, herein we developed this surface-initiated RAFT polymerization approach to synthesize narrowly distributed hollow nanocapsules using silica nanoparticles as sacrificial templates. The procedure is briefly presented in Scheme 1. After anchoring CTA onto the silica nanoparticles, a core−shell structure was realized by RAFT polymerization. Upon UV cross-linking of the polymer shell and dissolving the silica core in NH_4F/HF buffer solution, hollow nanocapsules were obtained. This approach, which employs RAFT as a very versatile controlled radical polymerization technique, demonstrates various advantages: (1) due to the availability of monodispersed silica nanoparticles, it is possible to synthesize nearly monodispersed hollow spheres with controlled size; (2) the composition of the capsules can be governed by choosing the desired functional monomers and CTA, e.g., RAFT polymerization has been used previously to synthesize well-defined biocompatible PEG acrylate,[68] HPMA,[69] and temperature-responsive NIPAAm polymers;[70] (3) the thickness of the shell can be modulated by simply controlling the molecular weight of grafted copolymer.

EXPERIMENTAL SECTION

Materials. 2,2′-Azobis(isobutyronitrile) (AIBN, Sigma, 98%) was recrystallized from methanol. *tert*-Butyl methacrylate (tBMA, Aldrich, 98%) was passed through an inhibitor removing column (neutral aluminum oxide) prior to being stored under an argon atmosphere in the refrigerator. Tetraethyl orthosilicate (TEOS, Sigma-Aldrich, 98%), 2-hydroxypropyl methacrylamide (HPMA, Aldrich, 99%), ammonia solution ($NH_3 \cdot H_2O$, Acros, 28 wt %), 4,4′-azobis(4-cyanovaleric acid) (ACVA, Sigma, 98%), 2-mercaptothiazoline (Sigma, 98%), methacryloyl chloride (Sigma, 97%), *N*,*N*′-dicyclohexylcarbodiimide (DCC, Fluka, 99%), 4-(dimethylamino)pyridine (DMAP, Aldrich 99%), aminopropyldimethylethoxysilane (abcr, 97%), and 2,3-dimethylmaleic anhydride (abcr, 97%) were used as received without further purification. The photo-cross-linker 2,3-dimethylmaleic imidopropyl methacrylate (DMIPM) was synthesized according to the methods in the literature,[71] as shown in the Supporting Information.

Synthesis of R-Group Activated 4-Cyanopentanoic Acid Dithiobenzoate (CPADB-ACPM).[72] The general synthetic route is shown in Scheme 2. A solution of 4,4′-azobis(4-cyanovaleric acid) (ACVA, 4.01 g, 14.3 mmol) and 2-mercaptothiazoline (4.50 g, 37.8 mmol) in 1,4-dioxane (200 mL) was degassed by nitrogen for 30 min. *N*,*N*′-Dicyclohexylcarbodiimide (DCC, 6.82 g, 33.0 mmol) and 4-(dimethylamino)pyridine (DMAP, 0.10 g, 0.82 mmol) dissolved in

dx.doi.org/10.1021/ma201982f |*Macromolecules* 2011, 44, 8351–8360

1,4-dioxane (100 mL) were added slowly at room temperature under rigorous stirring. After 20 h, the reaction mixture was filtered and concentrated. The product was precipitated in cold diethyl ether. After drying under vacuum, ACVA-ACPM was obtained as a yellow powder (5.96 g, 86.3% yield). ^{1}H NMR (500 MHz, $CDCl_3$): δ (ppm) 4.59 (t, 2H, NC**H**$_2$CH$_2$S), 3.31 (t, 2H, NCH$_2$C**H**$_2$S), 3.15−3.62 (m, 2H, (CN)C(CH$_3$)CH$_2$C**H**$_2$CON), 2.42−2.64 (m, 2H, (CN)C(CH$_3$)C**H**$_2$-CH$_2$CON), 1.76 (s, 3H, (CN)C(C**H**$_3$)CH$_2$). ^{13}C NMR (125 MHz, $CDCl_3$): δ (ppm) 201.9 (N**C**=S), 172.0 (CH$_2$**C**ON), 117.5 ((CH$_3$)-C(**C**N)CH$_2$), 72.0, 56.0, 34.0, 32.9, 28.4, 24.2.

Bis(thiobenzoyl) disulfide was synthesized according to the literature.[72] A solution of ACVA-ACPM (5.0 g, 10.3 mmol) and bis(thiobenzoyl) disulfide (2.5 g, 8.2 mmol) in ethyl acetate (250 mL) was heated at 80 °C for 20 h. After cooling, the reaction mixture was concentrated and purified by column chromatography (silica gel, 60−200 μm) using ethyl acetate/hexane (5/4, v/v) as eluent. R-group activated CPADB (CPADB-ACPM) was obtained as a red oil (3.5 g, 54.7%). ^{1}H NMR (500 MHz, $CDCl_3$): δ (ppm) 7.90 (d, 2H, phenyl group), 7.55 (t, 1H, phenyl group), 7.38 (t, 2H, phenyl group), 4.60 (t, 2H, NC**H**$_2$CH$_2$S), 3.60−3.66 (m, 2H, (CN)C(CH$_3$)CH$_2$C**H**$_2$CON), 3.32 (t, 2H, NCH$_2$C**H**$_2$S), 2.51−2.78 (m, 2H, (CN)C(CH$_3$)-C**H**$_2$CH$_2$CON), 1.94 (s, 3H, (C**H**$_3$)C(CN)S). ^{13}C NMR (125 MHz, $CDCl_3$): δ (ppm) 201.5 (NC=S), 172.1 (C=O), 144.6 (Ph), 132.9 (Ph), 128.6 (Ph), 126.7 (Ph), 118.6 (CN), 55.9, 45.7, 34.3, 33.3, 28.4, 24.2 (Figure S1, Supporting Information).

Preparation of Amino-Functionalized SNP. Uniform and monodisperse SNPs were synthesized according to the Stöber method.[73] Then a suspension (16 mL) of 10 wt % SNP was added to a round-bottom flask with 3-aminopropyldimethylethoxysilane (1.0 g, 6.0 mmol) and ammonium hydroxide solution (1 mL, 16 mmol). The reaction mixture was stirred at room temperature for 20 h. The particles were obtained by centrifugation of the reaction mixture at 3000 rpm for 5 min. Then the particles were thoroughly washed via centrifugation/redispersion cycles with ethanol for 5 times. The amino-functionalized SNP was dispersed directly into 50 mL of THF for subsequent use. An aliquot of the amino-functionalized SNP was dried and subjected to thermal gravimetric analysis (TGA) and elemental analysis to determine the amount of silane agent on the SNP (1.2 groups/nm^2).

Preparation of CTA Anchored Silica Nanoparticles. A THF solution of the amino-functionalized silica nanoparticles (25 mL, 4.0%) was added dropwise to a THF solution (30 mL) of R-group activated CTA (CPADB-ACPM) (1.0 mmol) at room temperature. After complete addition, the solution was stirred for another 6 h. The particles were recovered by centrifugation of the reaction mixture at 3000 rpm for 5 min followed by washing the particles with THF at least 5 times until the supernatant layer after centrifugation was colorless. Finally, the CTA anchored silica nanoparticles were dispersed in 1,4-dioxane for subsequent use.

RAFT Polymerization from CTA Anchored SNP. CTA anchored SNP (30 mg, 12 μmol CPADB/g), CPADB (4.5 mg, 16.1 μmol), 1,4-dioxane (3 mL), tBMA (400 mg, 2.81 mmol), and DMIPM (100 mg, 0.40 mmol) were added to a 10 mL of round-bottom flask followed by sonication and addition of AIBN (0.52 mg, 3.2 μmol). The flask was sealed, and the solution was purged with argon for 30 min before heating to 60 °C. After 13 h (conversion 45%), the solution was centrifuged and the particles were collected. The cycle of centrifugation and redispersion in 1,4-dioxane was repeated at least 5 times to ensure no free polymer remaining on the SNP surface. The product was dried in vacuo to yield a pink powder. After dissolving the silica core, the polymer obtained was characterized by ^{1}H NMR and GPC.

Chain Extension Based on PtBMA-*co*-PDMIPM Grafted SNP in the Presence of HPMA. The procedure for the chain extension of polyHPMA on the silica surface is described as follows: PtBMA-*co*-PDMIPM grafted SNP (50 mg, M_n of the grafted polymer 12 000 g/mol by GPC), HPMA monomer (200 mg, 1.4 mmol), CPADB (4.5 mg, 16.1 μmol), and 1,4-dioxane and ethanol (3 mL, v/v 50%) were added to a 10 mL round-bottom flask followed by sonication and addition of AIBN (0.52 mg, 3.2 μmol). The flask was sealed, and the solution was purged with argon for 30 min before heating to 60 °C. The polymerization was stopped by quenching in ice water, and the modified particles were washed by ethanol at least 5 times to ensure no free polymer remaining on the SNP surface. The block copolymer was obtained after dissolving the silica core and characterized by ^{1}H NMR and GPC.

Preparation of Hollow Nanocapsules. After the polymerization mentioned above, the core−shell structures were isolated from the solvent by centrifugation (30 mg) and placed in a 10 mL of flask with 4 mL of ethanol. The solution was sonicated for 30 min before UV light cross-linking. After exposure to UV light for 90 min (UVA Cube 100), the particles were recovered by centrifugation at 3000 rpm for 5 min. Then the inorganic silica core was etched by 8 M NH_4F/2 M HF buffer (pH ∼5): briefly, 30 mg of the block copolymer grafted SNP was stirred in 2 mL of NH_4F/HF buffer at room temperature for 12 h to dissolve the silica core. (*Caution*: HF is hazardous and very corrosive. Goggles and gloves must be worn during the operation.) The excess NH_4F, HF, and SiF_4 were removed from hollow nanospheres by dialysis in deionized water for 3 days. Finally, the hollow nanocapsules have been obtained by freeze-drying process.

Characterization Methods. The molecular weight distributions of the copolymers were measured at 40 °C using a Polymer Laboratories PL-GPC50 Plus Integrated GPC system (Varian Inc., UK) equipped with a Polymer Laboratories pump, a PL ResiPore column (300 × 7.5 mm), a PL data stream refractive index detector, and a PL-AS-RT autosampler. The calibration was carried out using 12 polystyrene standards with M_n values ranging from 162 to 371 100 (Varian Inc., UK). The eluent was THF, and the flow rate was 1.0 mL/min. The data were processed using Cirrus GPC offline GPC/SEC software (version 2.0).

^{1}H and ^{13}C NMR spectra were recorded using Bruker Avance III 500 spectrometer operating at 500.13 MHz (^{1}H) and 125.77 MHz (^{13}C), with $CDCl_3$ as solvent at room temperature.

The UV irradiation was carried out within a UVA Cube 100 (honle UV Technologies, Germany) equipped with an electrical input of the lamp of 100 W and a mercury lamp as UV source (200−700 nm). The distance between the sample and the lamp is 15 cm.

The confocal laser microscopy was carried out on Leica TCS SP5 confocal laser microscope system (Leica Microsystems, Wetzlar, Germany) with inverted Leica DMI6000 microscope stand and 40 × 1.25 oil immersion objective (excitation: 488 nm line of an argon laser). The nanocapsules were stained by Rose Bengal.

Fourier transform infrared (IR) spectroscopy analysis of the samples were carried out on a Bruker Equinox 55 Fourier transform infrared spectrophotometer, and the diffuse reflectance spectra were scanned over the range of 600−4000 cm^{-1} (resolution = 2 cm^{-1}, 100 scans per measurement). The samples were mixed with potassium bromide powder (≈4 mg sample/500 mg KBr) and background served as KBr powder.

X-ray photoelectron spectroscopy (XPS) measurements were made on an AXIS ULTRA (Kratos Analytical, England) spectrometer. The spectrometer was equipped with a monochromatic Al Kα ($h\nu$ = 1486.6 eV) X-ray source of 300 W at 15 kV. The kinetic energy of the photoelectrons was determined with a hemispheric analyzer set to pass energies of 160 eV for wide scan spectra and 20 eV for high-resolution spectra. During all measurements electrostatic charging of the sample was overcompensated by means of a low-energy electron source working in combination with a magnetic immersion lens. Later, all recorded peaks were shifted by the same amount which was necessary to set the C 1s peak to 285.00 eV for saturated hydrocarbons.

Thermogravimetric analysis (TGA) of the samples were carried on a TGA Q 5000 instrument (TA Instruments) The samples were heated

from room temperature to about 900 °C at a heating rate of 10 °C/min under a dry nitrogen atmosphere.

UV−vis measurements were done at Cary 100 scan (Varian Inc., UK) and Lambda 800 (Perkin-Elmer). They were carried out in a range from 700 to 400 nm using 1 nm steps.

The sizes and morphologies of the nanocapsules structure were observed using a transmission electron microscopy (TEM) Libra 120 at an accelerating voltage of 200 kV. The nanocapsules or particles were dispersed in water with the concentration of 1 mg/mL and deposited onto 300 mesh, carbon film coated copper grid, and the specimen was dried at room temperature. For the cryo-TEM measurement was conducted on the same instrument, except the sample was dispersed in Milli-Q water and frozen by liquid nitrogen. Scanning electron microscopy (SEM) images were obtained on a Zeiss Ultra 55 Gemini scanning electron microscope with the samples sputter-coated by 3 nm platinum.

DLS studies of 1 g/L aqueous nanocapsules solutions were carried out at 25 °C using a ZETASIZER Nano series instrument (Malvern Instruments, UK) equipped with a multipurpose autotitrator (MPT-2) and Dispersion Technology Software (version 4.00). The data were collected by the NIBS (noninvasive backscatter) method using a helium−neon laser (4 mW, λ = 632.8 nm) and a fixed angle of 173°.

RESULTS AND DISCUSSION

Synthesis of CTA Anchored SNP. Generally, the surface modification based on surface-initiated LRP techniques can be divided into two categories—"grafting to" and "grafting from" approaches—and both of them have advantages and limitations.[26] The "grafting to" approach can be straightforwardly used to graft well-defined prefabricated homopolymers and block copolymers to a substrate surface, except for the relatively low grafting densities due to steric repulsions. But this can be circumvented by the "grafting from" technique. The "grafting from" technique results in significantly higher grafting density because the steric barrier imposed by the in-situ grafted chains to incoming polymers does not limit the access of smaller monomer molecules to the active initiation sites. In this process, the surface of the particle is modified with a designed active initiation site monolayer followed by polymerization. Using the right system and techniques, one can control the functionality, density, and thickness of the polymer on the substrate,[26] and thus, we decided to focus on the grafting from approach to build up our polymer nanocapsules. In the surface-initiated RAFT process, the way of CTA immobilization on the surface of SNP is also crucial to synthesize well-defined grafted polymer. Normally CTA immobilization on surface can be performed using either (i) the R-group approach where the CTA is attached to the particles via the leaving and reinitiating R group or (ii) the Z-group approach where the CTA is attached to the particles via the stabilizing group.[64,67] Herein, we used the R-group approach ("grafting from") to synthesize grafted polymer on the surface of silica nanoparticles due to the fact that it can afford higher molecular weight and grafting density of the attached polymer. Also, the high grafting density is good to stabilize the hollow nanocapsules structure after the removal of the core.

Silica nanoparticles (SNP) were chosen as the sacrificial core material because monodisperse SiO_2 spheres can be easily synthesized by Stöber process, and the size and the monodispersity can be controlled by use of specific concentrations of water and ammonia.[73] In this study, the size of the used silica nanoparticles was about 440 nm (Figure S2, Supporting Information). Then the SiO_2 colloidal particle surfaces can be readily modified via commercially available silylating agents.

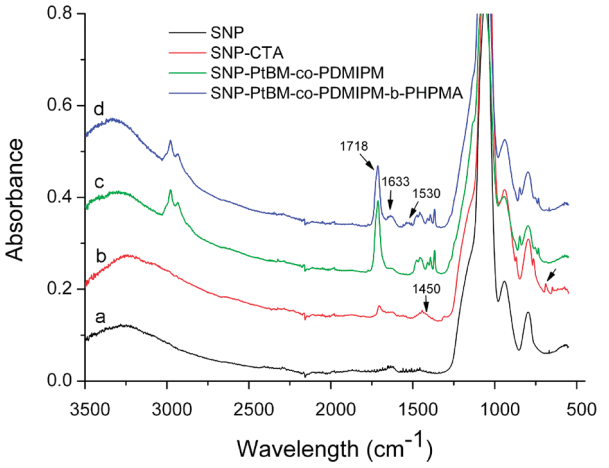

Figure 1. IR spectrum of (a) bare silica nanoparticles (SNP), (b) CTA anchored SNP, (c) PtBMA-*co*-PDMIPM copolymer grafted SNP, and (d) PtBMA-*co*-PDMIPM-*b*-PHPMA diblock copolymer grafted SNP.

As outlined in Scheme 1, the synthesized monodisperse SNP easily reacted with 3-aminopropyldimethylethoxysilane (APDMES) using NH_3 as catalyst to attach amino groups onto the surface. It should be mentioned that the NH_3 concentration is an important parameter for this reaction:[35] If it is too high, it will cause particle aggregation due to the high ionic strength. While if it is too low, it will make the reaction too slow. In this work, the final NH_3 concentration in the system was chosen to be 1 M. After reaction, the amino-functionalized SNP were thoroughly washed by repeating centrifugation and redispersion cycles in ethanol and water to remove the free amino group from the SNP surface. Followingly, to synthesize CTA anchored SNP, CTA dithioesters (CPADB) were first activated with 2-mercaptothiazoline on the carboxyl R-group. The reactivity of the mercaptothiazoline activated amide bond to selectively consume the amino groups in the presence of dithiobenzoate groups has been discussed by Benicewicz et al.[60] Although the CTA of dithioesters are susceptible to aminolysis even under mild conditions,[53,54,57] the reactivity of the mercaptothiazoline activated amide bond is sufficiently high to selectively consume the amino groups in the presence of dithiobenzoate groups. By dropwise addition of the amino-functionalized SNP solution to the R-group activated CTA solution, the CTA anchored SNP was obtained. Then, the solution was subjected to washing with THF until the supernatant layer after centrifugation was colorless for the subsequent use.

The attachment of CTA onto SNP was first confirmed by IR (Figure 1, curve b), which revealed the characteristic absorption bands at 1706 cm^{-1} attributed to the carbonyl group and at 1450 and 680 cm^{-1} due to the phenyl ring. The thiocarbonyl absorption at 1120 cm^{-1} was not observed due to the overlap with the strong absorption of bare silica. From the XPS (Figure S3a, Supporting Information), the specific peak of sulfur (S 2s, 225 eV) in CTA can be discerned. From UV−vis spectrometry of the CTA anchored SNP (Figure S4, curve c, Supporting Information), the characteristic peak of the CTA at 300 nm appeared. All of this strongly confirmed that the CTA was successfully anchored onto the SNP. Furthermore, the amount of CTA on the SNP was also determined quantitatively by comparing the absorption at 300 nm for the CTA anchored SNP to a standard absorption curve made from known amounts of the free CTA (the extinction coefficient of CTA (CPADB) at

300 nm is 15 000 L/(mol cm)). Together with elemental analysis and TGA results (Figure 2), it was revealed that the grafting density of CTA on the surface of SNP was 0.8 groups/nm^2, which is a little higher than the grafting density of RAFT CTAs (0.15−0.68 groups/nm^2) described in the literature.[61,67]

Growing Core−Shell Structure by Surface-Initiated RAFT Polymerization. Surface-initiated RAFT polymerization onto SNP was initially performed employing *tert*-butyl methacrylate (tBMA) and 2,3-dimethylmaleic imidopropyl methacrylate (DMIPM) as monomers in the presence of free CTA. The monomer DMIPM was employed to enhance later on the stability of nanocapsules by photo-cross-linking. Polymerization was conducted in 1,4-dioxane at 60 °C for 13 h with the final molar ratio $[tBMA]_0/[DMIPM]_0/[CTA]_0/[initiator]_0$ of 170:24:1.0:0.2. Free CTA was added in the system in order to slow down the propagation of free chains in solution and favor the addition−fragmentation reactions on solid support.[60] After polymerization, the PtBMA-*co*-PDMIPM grafted SNP were extensively purified by repeating the cycle of centrifugation and redispersion in 1,4-dioxane to remove the nongrafted polymer from the particles. The appearance of the new absorption bands at 1727 cm^{-1} (carbonyl peak) in the IR spectra (Figure 1c) and the characteristic peak of 400 eV (N 1s) and 282 eV (C 1s) in the XPS (Figure S3b, Supporting Information) well confirmed that the copolymer was grafted onto silica nanoparticles. In the TGA analysis, these hybrid particles underwent an additional 3% weight loss due to the presence of the copolymer, and combined with elemental analysis, the grafting density was determined to be about 0.32 polymer chain per nm^2 (assuming the density of the silica nanoparticle 2.07 g/cm^3).[60] Giving the steric hindrance between the polymer chains and that not all the CTA on the silica surface can be validated to grow polymer, the slight decrease of the copolymer graft density compared to that of CTA is reasonable. The SEM and TEM images of the copolymer grafted SNP (M_n of the grafted polymer 12 000 g/mol, PDI 1.20, by GPC, entry 1 in Table 1) are shown in parts c and d of Figure 3, respectively. Both images demonstrate the highly uniform spherical morphology with the size of about 450 nm. In the comparison of TEM images before (Figure 3b) and after (Figure 3d) polymerization, a shell structure can be discerned on the silica particle after polymerization in Figure 3d (inset) with a uniform thickness of the shell of

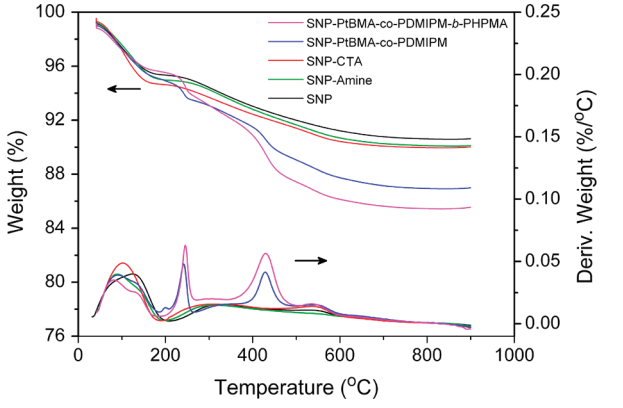

Figure 2. TGA curves of (a) bare silica nanoparticle (SNP), (b) amino-functionalized SNP, (c) CTA anchored SNP, (d) PtBMA-*co*-PDMIPM grafted SNP, and (e) PtBMA-*co*-PDMIPM-*b*-PHPMA grafted SNP.

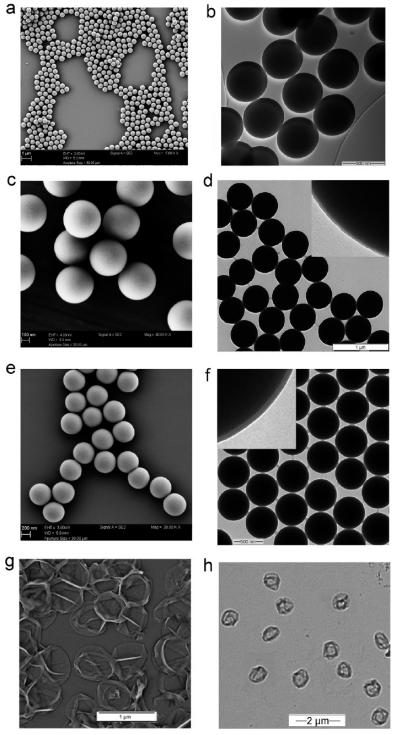

Figure 3. (a) SEM and (b) TEM images of CTA anchored SNP, (c) SEM and (d) TEM images of PtBM-*co*-PDMIPM grafted SNP (M_n of the grafted copolymer 12 000 g/mol, PDI 1.20 by GPC), (e) SEM and (f) TEM images of PtBM-*co*-PDMIPM-*b*-PHPMA grafted SNP (M_n of the grafted block copolymer 19 500 g/mol, PDI 1.30 by GPC), (g) SEM and (h) TEM images of PtBMA-*co*-PDMIPM-*b*-PHPMA nanocapsules (silica nanoparticles dissolved with NH_4/HF buffer).

Table 1. Characterization of the Grafted Polymers in This Study

entry	sample[a]	M_n of grafted polymer[b] (g/mol)	PDI[b]	shell thickness[c] (nm)	grafting density[d] (chains/nm^2)	DP$_n$[e] (DMIPM)
1	SNP-PtBM-*co*-PDMIPM	12 000	1.20	5.0	0.32	10
2	SNP-PtBM-*co*-PDMIPM-*b*-PHPMA	19 500	1.30	10.0	0.22	10
3	SNP-PtBM-*co*-PDMIPM 1	5 000	1.23	3.0	ND[f]	4
4	SNP-PtBM-*co*-PDMIPM 2	9 500	1.18	4.8	ND	9
5	SNP-PtBM-*co*-PDMIPM 3	19 000	1.16	8.2	ND	15

[a] Silica nanoparticles of 440 nm were used as the template. [b] Number-average molecular weight (M_n) and polydispersity index (PDI) of the grafted polymer were determined by GPC (polystyrene calibration). [c] The thickness of the core−shell structure was measured by TEM. [d] The grafting density of the polymer on the silica nanoparticles was calculated by elemental analysis. [e] DP$_n$ (DMIPM) corresponds to average number of polymerization of (DMIPM) in the copolymer chain calculated by ^{1}H NMR. [f] ND means not detected.

dx.doi.org/10.1021/ma201982f |*Macromolecules* 2011, 44, 8351–8360

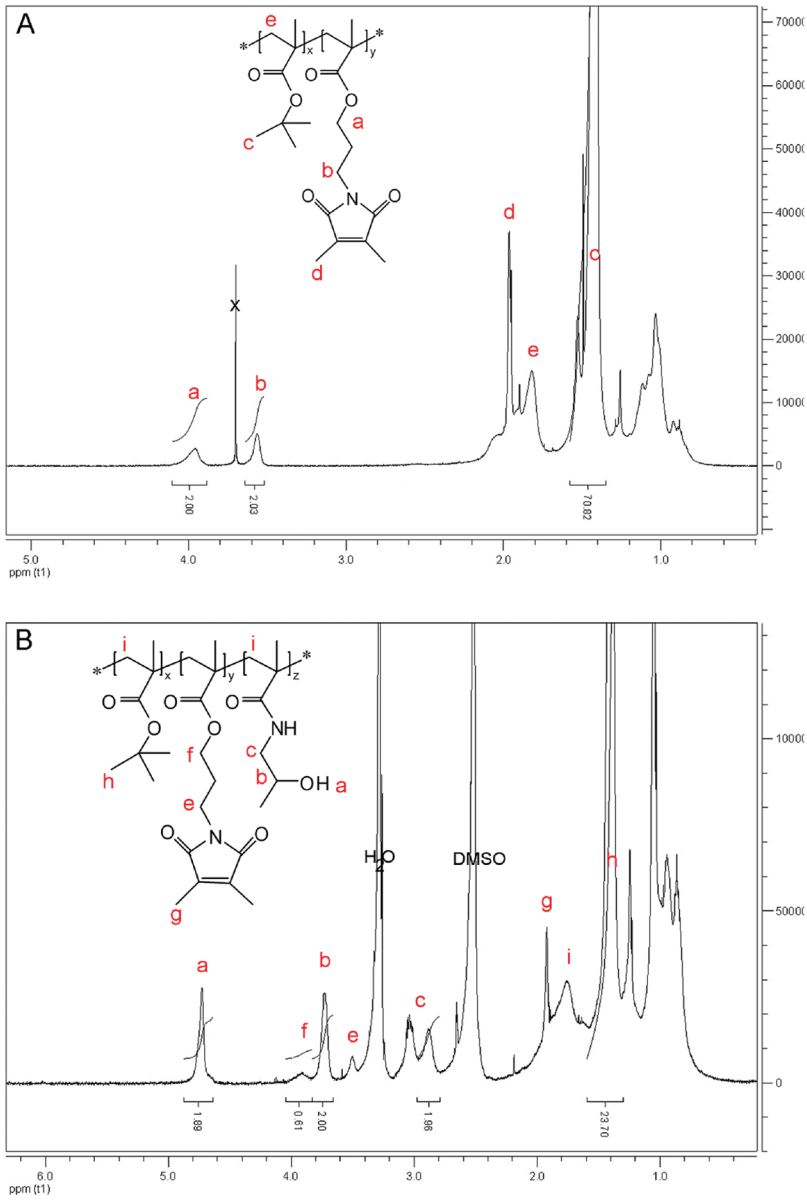

Figure 4. ^{1}H NMR spectra of the grafted (A) copolymer PtBMA-*co*-PDMIPM and (B) block copolymer PtBMA-*co*-PDMIPM-*b*-PHPMA. Both grafted copolymers were obtained by etching out the modified silica nanoparticle with NH_4F/HF buffer.

about 5 nm, and the magnified TEM image was shown in Figure S6a (Supporting Information).

In addition, treating the copolymer grafted SNP with NH_4F/HF buffer, the grafted copolymer (PtBMA-*co*-PDMIPM) was collected and further analyzed by GPC and ^{1}H NMR (entry 1 in Table 1). Figure 4A shows the ^{1}H NMR spectrum of the grafted copolymer PtBMA-*co*-PDMIPM. Every characteristic hydrogen signal of the two monomers, tBMA and DMIPM, can be found in the polymer chain, indicating the copolymerization took place. Furthermore, the content of PDMIPM in the copolymer chain was calculated to be about 11.5% by the integration ratio between the specific signals of DMIPM at 3.96 ppm and tBMA at 1.5 ppm, respectively. From GPC, the number-averaged molecular weight of the grafted copolymer (PtBMA-*co*-PDMIPM) was determined to be 12 000 g/mol with a PDI of 1.20. In comparison with a free polymer, the grafted polymer was found to demonstrate slightly lower molecular weight and slightly broader PDI (Figure S5, Supporting Information). Similar behavior was also observed and explained for surface-initiated ATRP.[28]

Furthermore, to study if the molecular weight and polydispersity of the grafted copolymer can be well controlled by the surface-initiated RAFT polymerization, a simple kinetics study for tBMA and DMIPM copolymerization mediated by the CTA anchored SNP was conducted. The graph in Figure 5 shows an almost linear relationship between monomer consumption and time for all four cases, which indicates a constant free radical concentration during the polymerization. Furthermore, while the reaction proceeded, the molecular weights increased nearly linearly and the molecular weight distributions remained narrow (PDI $\leq$ 1.30). This indicates a controlled polymerization. Accordingly, it is assumed that for the copolymer grafted core−shell structure the thickness of the shell could be governed by the molecular weight of the grafted copolymer. As shown in Figure 6a−c, different thickness of the shell (3.0, 4.8, and 8.2 nm) around the silica nanoparticles

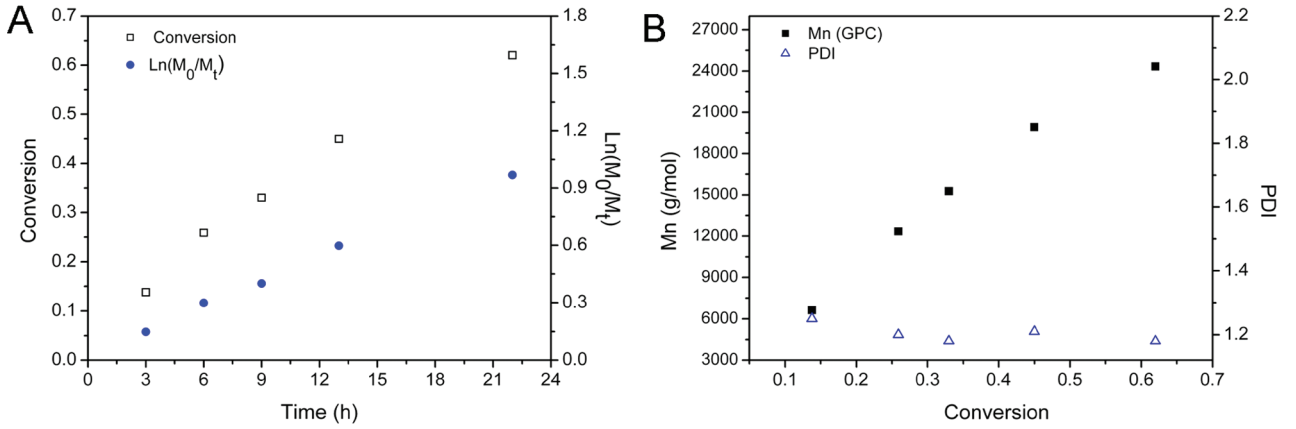

Figure 5. Surface-initiated RAFT copolymerization of tBMA and DMIPM was conducted in 1,4-dioxane at 60 °C with final molar ratio of $[tBMA]_0/[DMIPM]_0/[CTA]_0/[AIBN]_0$ = 300/100/1/0.2: (A) polymerization kinetic plots: monomer conversion versus time and $\ln([M]_0/[M]$ versus time); (B) evolution of the number-average molecular weight (M_n) determined by GPC and polydispersity index (PDI) versus conversion. The grafted copolymer was recovered by treating the purified copolymer grafted SNP in NH_4F/HF buffer.

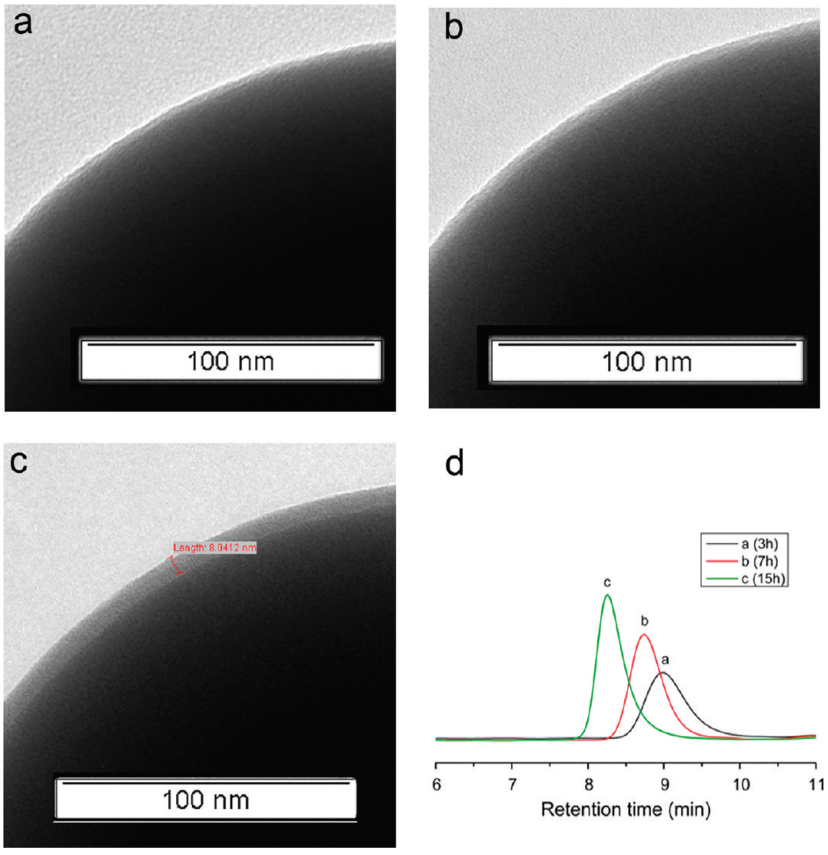

Figure 6. (a, b, and c) TEM images of PtBMA-*co*-PDMIPM grafted SNP with different reaction times of 3, 7, and 15 h, respectively. (d) The corresponding GPC traces of the grafted copolymers after etching out the SNP (entries 3, 4, and 5, in Table 1).

were obtained by controlling the polymerization time. The molecular weight of the grafted copolymer (recovered by treating the purified copolymer grafted SNP in NH_4F/HF buffer) was measured by GPC (Figure 6d), clearly indicating that the longer reaction time resulted in a higher molecular weight of the grafted copolymer which leads to the increase in the thickness of the shell.

Having successfully obtained the copolymer (PtBMA-*co*-PDMIPM) grafted SNP, chain extension was performed further on the surface based on the PtBMA-*co*-PDMIPM grafted SNP as macroCTA and HPMA as monomer under the same conditions. After polymerization, the block copolymer (PtBMA-*co*-PDMIPM-*b*-PHPMA) grafted SNP was purified by at least five times centrifugation/redispersion cycles in ethanol and subsequently characterized. Figure 1d shows the IR spectra of the block copolymer grafted SNP. The new adsorption peaks of amide (C═O) at 1633 cm^{-1} and the N−H bending mode bands

dx.doi.org/10.1021/ma201982f |*Macromolecules* 2011, 44, 8351–8360

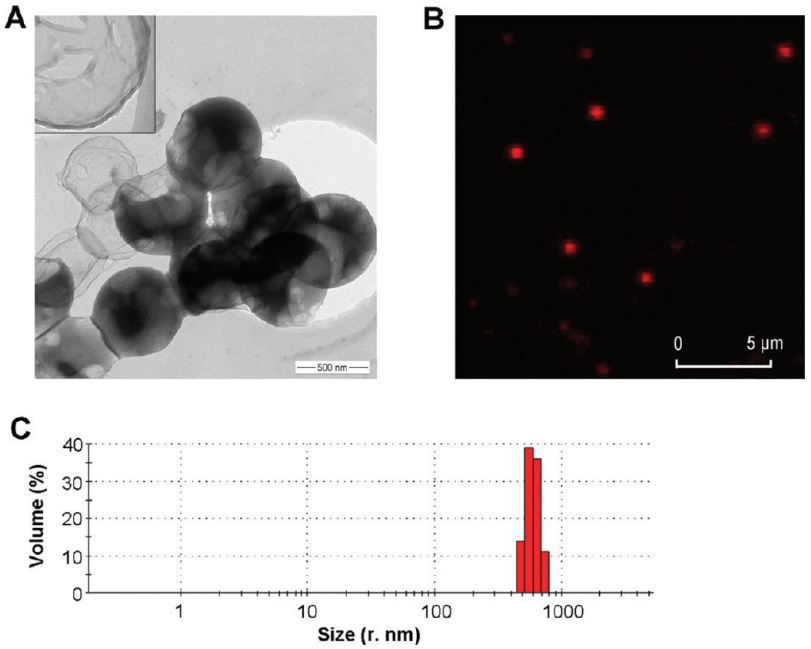

Figure 7. (A) Cryo-TEM and (B) laser confocal microscopy images of PtBMA-*co*-PDMIPM-*b*-PHPMA nanocapsules (M_n of the block copolymer 19 500 g/mol, GPC). (C) Dynamic light scattering data of the nanocapsules with the concentration of 1 mg/mL in Milli-Q water.

at about 1530 cm^{-1} indicated the presence of PHPMA chain. TGA analysis of the block copolymer (PtBMA-*co*-PDMIPM-*b*-PHPMA) grafted SNP showed an additional 1.5% weight loss compared with PtBMA-*co*-PDMIPM grafted SNP. This also confirms the presence of the PHPMA chain. Together with elemental analysis, grafting density of the second block chain PHPMA on SNP was calculated to be about 0.22 polymer chain/nm^2. In addition, after treating the block copolymer grafted silica nanoparticles with NH_4F/HF buffer, the recovered block copolymer was further analyzed by GPC and ^{1}H NMR as summarized in Table 1. From the GPC it was confirmed that the number-average molecular weight increased from 12 000 g/mol for the grafted copolymer to 19 500 g/mol with PDI of 1.30 for the grafted block copolymer. By calculating the integration ratio of the specific ^{1}H NMR signals of DMIPM at 3.96 ppm, tBMA at 1.5 ppm, and HPMA at 3.75 ppm, in the ^{1}H NMR spectrum (Figure 4B), the number of monomer units of DMIPM, tBMA, and HPMA in the copolymer chains was determined to be 10, 66, and 50, respectively. Moreover, after chain extension there was an obvious increase on the thickness of the shell (10 nm) as deduced from the TEM images (Figure 3f, inset) compared with that before chain extension (5 nm) (Figure 3d, inset) (the more magnified images are also shown in Figure S6, Supporting Information), which again indicates that the second polymer chain PHPMA was successfully attached on the copolymer shell of the silica nanoparticles.

Preparation of Polymeric Nanocapsules. Normally, to ensure the integrity of nanocapsules after the removal of the template, a cross-linking strategy has to be employed, and this can be achieved using a number of alternative approaches; for example, click reactions,[74] carbodiimide reactions (amine−acid reactions),[19,24] activated ester−amine reactions,[75] photoinduced reactions,[16] and disulfide-based reactions[9] have been reported. In this study, the photo-cross-linker (DMIPM), which had been demonstrated in our group's previous work to be effective for polymersome cross-linking, was exploited.[16] Exposure of the prepared PtBMA-*co*-PDMIPM-*b*-PHPMA grafted SNP under the unfiltered light of a mercury lamp for 90 min gave a cross-linked shell on the surface of SNP due to the dimethylmaleimide moieties in PDMIPM chains forming dimers. By subsequent etching out the silica nanoparticles in NH_4F/HF buffer, hollow polymeric nanocapsules were produced. It should be noted that, without photo-cross-linking, after etching out the core, no nanocapsule structure was formed. A comparison of XPS spectra taken before and after reaction with the HF buffer indicated the loss of silica nanoparticle and the retention of the polymeric component (Figure S3d, Supporting Information). The formation of hollow polymeric nanocapsules was supported first by SEM and standard TEM analysis. The TEM images are shown in Figure 3h, from which the hollow polymeric nanocapsules with uniform size of about 450 nm can be clearly identified as collapsed structure. Furthermore, the collapsed structure shown in the SEM images (Figure 3g) is also given due to the fact that the relative thin and flexible shell was not strong enough to sustain the hollow spherical structure after drying. To further confirm the hollow sphere structure, cryo-TEM measurements were conducted to observe the real morphology of the nanocapsules in solution. As seen in Figure 7A, the globular structure of the nanocapsules can be clearly observed, and the darker areas inside the nanocapsules are due to the presence of frozen water. Also from the magnified image (Figure 7A, inset), the shell of the nanocapsules is identified with a thickness of about 10 nm, which is accordance with the results obtained on the particles before the dissolution of the silica core. From the laser confocal microscopy image (Figure 7B) the spherical morphology of the nanocapsule can also been observed, but due to the resolution limitation of the device, the hollow structure cannot been further discerned. Finally, from dynamic light scattering (DLS), the polydispersity index (PDI) and diameter of the nanocapsules have been determined to be 0.119 and 553 nm, respectively. Compared with the data obtained by SEM or standard TEM, the slight increase in diameter in DLS is normal, considering the contribution from the swollen corona of the nanocapsules in solution.

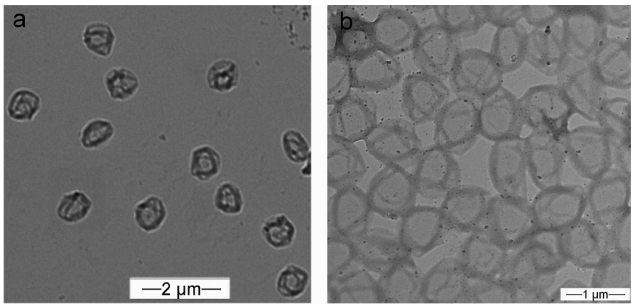

Figure 8. TEM images of (a) 450 nm and (b) 900 nm PtBMA-*co*-PDMIPM-*b*-PHPMA hollow nanocapsules.

Similar as the thickness of the shell can be easily regulated by controlling the molecular weight of the grafted polymer, the size of the hollow nanocapsules can also be simply varied by using different size of SNP as templates. As shown in Figure 8, a different size of the hollow nanocapsule (900 nm) was also prepared by using a corresponding size of SNP as template under the same procedure.

Finally, in order to confirm that the polymeric shell of the capsules should be still intact after degradation of the silica core, a control experiment was conducted to investigate the effect of the NH_4F/HF buffer solution on the ester bonds of the monomers DMIPM, tBMA, and HPMA. Each monomer was exposed to the buffer solution for 2 days longer than the conditions used for the dissolution of nanoparticle. After extracting the monomer from buffer solution, ^{1}H NMR analyses showed that all monomers were unaffected by this treatment.

CONCLUSIONS

In this work we could demonstrate the successful synthesis of hollow nanocapsules by surface-initiated RAFT polymerization using silica nanoparticles as sacrificial templates. A photo-cross-linker moiety in the polymer shell was used to stabilize the nanocapsules. Combining TEM, SEM, cryo-TEM, DLS, ^{1}H NMR, GPC, IR, XPS, and TGA analysis, the chemical composition and morphology and shape of the nanocapsules were fully confirmed. Furthermore, the size of the nanocapsules, the composition, and the thickness of the shell can be easily governed by choosing silica templates of different size, functional comonomers, and by controlling the molecular weight of grafted polymer. Here, considering these good virtues, by choosing properly functional monomers, a nontoxic and biocompatible nanocapsule is possible to reach in future based on the surface-initiated RAFT polymerization method, and once applied in the field of the controlled biomolecules (drugs/siRNA) release, it will be a promising vehicle, especially considering that the release behavior can be mediated by both external stimuli such as temperature, pH or redox, and internal parameters such as the thickness of the shell or the degree and nature of cross-linking. Furthermore, the narrow size distribution of the hollow spheres governed by the template is expected to lead to more uniform physical and chemical properties, thereby making it easier, for example, to formulate a more sophisticated drug delivery system or to study the interaction with biology. As the RAFT chemistry employed is very compatible with biological conditions and since a variety of biocompatible as well as bioactive monomers can be incorporated into the polymer shell of our nanocapsules by that process, we see further advantages of this approach. Presently, a hollow nanocapsule based on the described approach having a degradable as well as pH-sensitive polymer shell is under investigation in our group.

ASSOCIATED CONTENT

Supporting Information. Synthesis procedure of the photo-cross-linker, NMR data for CTA, GPC and XPS data for the grafted polymer and modified SNP, and magnified TEM images of the core shell structure. This material is available free of charge via the Internet at http://pubs.acs.org.

AUTHOR INFORMATION

Corresponding Authors

*E-mail: huang@ipfdd.de (X.H.), appelhans@ipfdd.de (D.A.). Tel: 49-351-4658353. Fax: 49-351-4658565.

ACKNOWLEDGMENT

X. Huang is grateful for the fellowship from the Alexander von Humboldt Foundation. The authors also thank Maria Auf der Landwehr, Uta Reuter, Franka Ennen, Martin Kaufmann, Liane Häussler, and Mohamed Yassin for their help with SEM, TEM, laser confocal microscopy, TGA, and DLS, and all other colleagues who contributed the work.

REFERENCES

(1) Shi, X.; Shen, M.; Möhwald, H. *Prog. Polym. Sci.* **2004**, *29*, 987–1019.
(2) Chong, S. F.; Lee, J. H.; Zelikin, A. N.; Caruso, F. *Langmuir* **2011**, *27*, 1724–1730.
(3) Kim, K. T.; Cornelissen, J. J. L. M.; Nolte, R. J. M.; van Hest, J. *Adv. Mater.* **2009**, *21*, 2787–2791.
(4) Jiang, P.; Bertone, J. F.; Colvin, V. L. *Science* **2001**, *291*, 453–457.
(5) Ding, J.; Liu, G. *J. Phys. Chem. B* **1998**, *102*, 6107–6113.
(6) Shchukin, D. G.; Shutava, T.; Shchukina, E.; Sukhorukov, G. B.; Lvov, Y. M. *Chem. Mater.* **2004**, *16*, 3446–3451.
(7) Kim, S. W.; Kim, M.; Lee, W. Y.; Hyeon, T. *J. Am. Chem. Soc.* **2002**, *124*, 7642–7643.
(8) Xu, X.; Asher, S. A. *J. Am. Chem. Soc.* **2004**, *126*, 7940–7945.
(9) Chandrawati, R.; Städler, B.; Postma, A.; Connal, L. A.; Chong, S. F.; Zelikin, A. N.; Caruso, F. *Biomaterials* **2009**, *30*, 5988–5998.
(10) Städler, B.; Price, A. D.; Zelikin, A. N. *Adv. Funct. Mater.* **2011**, *21*, 14–28.
(11) Limer, A.; Gayet, F.; Jagielski, N.; Heming, A.; Shirley, I.; Haddleton, D. M. *Soft Matter* **2011**, *7*, 5408–5416.
(12) Wu, C.; Wang, X.; Zhao, L.; Gao, Y.; Ma, R.; An, Y.; Shi, L. *Langmuir* **2010**, *26*, 18503–18507.
(13) van Dongen, S. F. M.; Nallani, M.; Schoffelen, S.; Cornelissen, J. J. L. M.; Nolte, R. J. M.; van Hest, J. *Macromol. Rapid Commun.* **2008**, *29*, 321–325.
(14) De Geest, B. G.; Van Camp, W.; Du Prez, F. E.; De Smedt, S. C.; Demeester, J.; Hennink, W. E. *Chem. Commun.* **2008**, 190–192.
(15) He, W. D.; Sun, X. L.; Wan, W. M.; Pan, C. Y. *Macromolecules* **2011**, *44*, 3358–3365.
(16) Gaitzsch, J.; Appelhans, D.; Gräfe, D.; Schwille, P.; Voit, B. *Chem. Commun.* **2011**, *47*, 3466–3468.
(17) Landfester, K.; Musyanovych, A.; Mailänder, V. *J. Polym. Sci., Part A: Polym. Chem.* **2010**, *48*, 493–515.
(18) Paiphansiri, U.; Tangboriboonrat, P.; Landfester, K. *Macromol. Biosci.* **2006**, *6*, 33–40.
(19) O'Reilly, R. K.; Joralemon, M. J.; Hawker, C. J.; Wooley, K. L. *J. Polym. Sci., Part A: Polym. Chem.* **2006**, *44*, 5203–5217.

(20) McCormick, C. L.; Sumerlin, B. S.; Lokitz, B. S.; Stempka, J. E. *Soft Matter* **2008**, *4*, 1760–1773.
(21) Rimmer, S.; Carter, S.; Rutkaite, R.; Haycock, J. W.; Swanson, L. *Soft Matter* **2007**, *3*, 971–973.
(22) Xu, J.; Tao, L.; Boyer, C.; Lowe, A. B.; Davis, T. P. *Macromolecules* **2011**, *44*, 299–312.
(23) Wang, Y.; Angelatos, A. S.; Caruso, F. *Chem. Mater.* **2007**, *20*, 848–858.
(24) Boyer, C.; Whittaker, M. R.; Nouvel, C.; Davis, T. P. *Macromolecules* **2010**, *43*, 1792–1799.
(25) Ochs, C. J.; Such, G. K.; Yan, Y.; van Koeverden, M. P.; Caruso, F. *ACS Nano* **2010**, *4*, 1653–1663.
(26) Radhakrishnan, B.; Ranjan, R.; Brittain, W. J. *Soft Matter* **2006**, *2*, 386–396.
(27) Matyjaszewski, K.; Tsarevsky, N. V. *Nature Chem.* **2009**, *1*, 276–288.
(28) von Werne, T.; Patten, T. E. *J. Am. Chem. Soc.* **2001**, *123*, 7497–7505.
(29) Shah, R. R.; Merreceyes, D.; Husemann, M.; Rees, I.; Abbott, N. L.; Hawker, C. J.; Hedrick, J. L. *Macromolecules* **2000**, *33*, 597–605.
(30) Ejaz, M.; Ohno, K.; Tsujii, Y.; Fukuda, T. *Macromolecules* **2000**, *33*, 2870–2874.
(31) Pi, M.; Yang, T.; Yuan, J.; Fujii, S.; Kakigi, Y.; Nakamura, Y.; Cheng, S. *Colloids Surf., B* **2010**, *78*, 193–199.
(32) Hubner, E.; Allgaier, J.; Meyer, M.; Stellbrink, J.; Pyckhout-Hintzen, W.; Richter, D. *Macromolecules* **2009**, *43*, 856–867.
(33) Wen, F.; Zhang, W.; Zheng, P.; Zhang, X.; Yang, X.; Wang, Y.; Jiang, X.; Wei, G.; Shi, L. *J. Polym. Sci., Part A: Polym. Chem.* **2008**, *46*, 1192–1202.
(34) Radhakrishnan, B.; Constable, A. N.; Brittain, W. J. *Macromol. Rapid Commun.* **2008**, *29*, 1828–1833.
(35) Ohno, K.; Morinaga, T.; Koh, K.; Tsujii, Y.; Fukuda, T. *Macromolecules* **2005**, *38*, 2137–2142.
(36) Li, D.; Sheng, X.; Zhao, B. *J. Am. Chem. Soc.* **2005**, *127*, 6248–6256.
(37) Pyun, J.; Jia, S.; Kowalewski, T.; Patterson, G. D.; Matyjaszewski, K. *Macromolecules* **2003**, *36*, 5094–5104.
(38) Jiang, X.; Zhao, B.; Zhong, G.; Jin, N.; Horton, J. M.; Zhu, L.; Hafner, R. S.; Lodge, T. P. *Macromolecules* **2010**, *43*, 8209–8217.
(39) Ejaz, M.; Tsujii, Y.; Fukuda, T. *Polymer* **2001**, *42*, 6811–6815.
(40) Yao, Z.; Braidy, N.; Botton, G. A.; Adronov, A. *J. Am. Chem. Soc.* **2003**, *125*, 16015–16024.
(41) Baskaran, D.; Mays, J. W.; Bratcher, M. S. *Angew. Chem., Int. Ed.* **2004**, *43*, 2138–2142.
(42) Blomberg, S.; Ostberg, S.; Harth, E.; Bosman, A. W.; Van Horn, B.; Hawker, C. J. *J. Polym. Sci., Part A: Polym. Chem.* **2002**, *40*, 1309–1320.
(43) Li, G. L.; Xu, L. Q.; Tang, X.; Neoh, K.; Kang, E. *Macromolecules* **2010**, *43*, 5797–5803.
(44) Chen, F.; Jiang, X.; Liu, R.; Yin, J. *Polym. Chem.* **2011**, *2*, 614–618.
(45) Zhou, K.; Tong, L.; Deng, J.; Yang, W. *J. Mater. Chem.* **2009**, *20*, 781–789.
(46) Liu, G.; Zhang, H.; Yang, X.; Wang, Y. *J. Appl. Polym. Sci.* **2009**, *111*, 1964–1975.
(47) Ji, H.; Wang, S.; Yang, X. *Polymer* **2009**, *50*, 133–140.
(48) Li, G.; Lei, C.; Wang, C.; Neoh, K.; Kang, E.; Yang, X. *Macromolecules* **2008**, *41*, 9487–9490.
(49) Fu, G.; Shang, Z.; Hong, L.; Kang, E.; Neoh, K. *Macromolecules* **2005**, *38*, 7867–7871.
(50) Ali, M. M.; Stöver, H. D. H. *Macromolecules* **2003**, *36*, 1793–1801.
(51) Morinaga, T.; Ohkura, M.; Ohno, K.; Tsujii, Y.; Fukuda, T. *Macromolecules* **2007**, *40*, 1159–1164.
(52) Ali, S. I.; Heuts, J. P. A.; van Herk, A. M. *Soft Matter* **2011**, *7*, 5382–5390.
(53) Boyer, C.; Stenzel, M. H.; Davis, T. P. *J. Polym. Sci., Part A: Polym. Chem.* **2011**, *49*, 551–595.
(54) Boyer, C.; Bulmus, V.; Davis, T. P.; Ladmiral, V.; Liu, J.; Perrier, S. *Chem. Rev.* **2009**, *109*, 5402–5436.
(55) Barner-Kowollik, C. *Angew. Chem., Int. Ed.* **2009**, *48*, 9222–9224.
(56) Moad, G.; Rizzardo, E.; Thang, S. H. *Acc. Chem. Res.* **2008**, *41*, 1133–1142.
(57) Moad, G.; Rizzardo, E.; Thang, S. H. *Polymer* **2008**, *49*, 1079–1131.
(58) Semsarilar, M.; Perrier, S. *Nature Chem.* **2010**, *2*, 811–820.
(59) Mitsukami, Y.; Donovan, M. S.; Lowe, A. B.; McCormick, C. L. *Macromolecules* **2001**, *34*, 2248–2256.
(60) Li, C.; Han, J.; Ryu, C. Y.; Benicewicz, B. C. *Macromolecules* **2006**, *39*, 3175–3183.
(61) Li, C.; Benicewicz, B. C. *Macromolecules* **2005**, *38*, 5929–5936.
(62) Ranjan, R.; Brittain, W. J. *Macromolecules* **2007**, *40*, 6217–6223.
(63) Ranjan, R.; Brittain, W. J. *Macromol. Rapid Commun.* **2008**, *29*, 1104–1110.
(64) Zhao, Y.; Perrier, S. *Macromolecules* **2006**, *39*, 8603–8608.
(65) Huang, Y.; Hou, T.; Cao, X.; Perrier, S.; Zhao, Y. *Polym. Chem.* **2010**, *1*, 1615–1623.
(66) Hong, C. Y.; Li, X.; Pan, C. Y. *Eur. Polym. J.* **2007**, *43*, 4114–4122.
(67) Perrier, S.; Takolpuckdee, P.; Mars, C. A. *Macromolecules* **2005**, *38*, 6770–6774.
(68) Roth, P. J.; Jochum, F. D.; Zentel, R.; Theato, P. *Biomacromolecules* **2010**, *11*, 238–244.
(69) Tao, L.; Xu, J.; Gell, D.; Davis, T. P. *Macromolecules* **2010**, *43*, 3721–3727.
(70) Huang, X.; Boyer, C.; Davis, T. P.; Bulmus, V. *Polym. Chem.* **2011**, *2*, 1505–1512.
(71) Kuckling, D.; Vo, C. D.; Adler, H. J. P.; Völkel, A.; Cölfen, H. *Macromolecules* **2006**, *39*, 1585–1591.
(72) Xu, J.; Boyer, C.; Bulmus, V.; Davis, T. P. *J. Polym. Sci., Part A: Polym. Chem.* **2009**, *47*, 4302–4313.
(73) Stöber, W.; Fink, A.; Bohn, E. *J. Colloid Interface Sci.* **1968**, *26*, 62–69.
(74) Kinnane, C. R.; Such, G. K.; Caruso, F. *Macromolecules* **2011**, *44*, 1194–1202.
(75) Fang, H.; Zhang, K.; Shen, G.; Wooley, K. L.; Taylor, J. S. A. *Mol. Pharmaceutics* **2009**, *6*, 615–626.